Ocean Engineering 124 (2016) 42–53

Contents lists available at ScienceDirect

Ocean Engineering

journal homepage: www.elsevier.com/locate/oceaneng

A study on the heave performance and loads of the critical connections of a novel dry tree semisubmersible concept using numerical and experimental methods

Zhe Jiang [a,*], Bin Xie [b], Weicheng Cui [a], Qinggui Du [b], Xinliang Tian [c]

[a] Hadal Science and Technology Research Center (Shanghai Engineering Research Center of Hadal Science and Technology), Shanghai Ocean University, No. 999 Hucheng Huan Road, Shanghai, 201306 China
[b] General Research Institute, China National Offshore Oil Corporation, No. 8 South Taiyanggong Street, CNOOC Plaza, Beijing, 100028 China
[c] State Key Laboratory of Ocean Engineering, Shanghai Jiaotong University, No. 800 Dongchuan Road, 200240, China

ARTICLE INFO

Article history:
Received 23 August 2015
Received in revised form
17 May 2016
Accepted 16 July 2016

Keywords:
Deepwater tumbler platform
Double tier pontoons
Heave performance
Numerical simulation
Model test

ABSTRACT

Deepwater tumbler platform (DTP) is a novel semisubmersible concept in offshore industry, which utilizes double tier pontoons to improve heave performance so as to support dry tree systems, and to enable the platform stable unconditionally by installing ballast in lower tier pontoons (LTPs). However, the effectiveness of double tier pontoons on reducing heave motions has not been extensively studied, and additionally, the weight of LTPs brings in extra structural loads on the connections between the upper tier pontoons and LTPs, which make this connection the most critical one in the design of DTP. Therefore, the heave performance and the loads of the connections are the two main concerns in developing the DTP concept. In this paper, the hydrodynamic behavior of DTP and the loads of the connections are analyzed by numerical simulations as well as model tests. Good agreement of the numerical results with the experimental measurements was found and the results of both prove that the design of double tier pontoons greatly improves the heave performance. Besides, considerable amount of forces and bending moments by the motions of LTP were exerted on the connections. Finally, through a sensitivity study on the LTP depth, the relationship among LTP depth, heave performance and connection loads were discovered. This study illustrates the use of double tier pontoons in improving heave performance and provides important design guidance on the DTP design.

1. Introduction

The potential application of a dry tree system on a semisubmersible floating production platform have attracted much interests in recent years and spawned many novel concepts in the offshore oil & gas industry. Oil and gas production may originate from wellheads on the sea floor (wet trees), or from wellheads located on the platform (dry trees). Comparing with the wet tree system, the dry tree system has many advantages such as efficient drilling and workover, low operation cost, short downtime and favorable flow assurance, etc. Normally, the application of dry tree systems has strict restrictions in heave responses, which conventional semisubmersibles (semis) can hardly satisfy. In such circumstances, many efforts have been made to decrease the heave responses of semis so as to support dry tree systems.

The heave responses are more governed by wave frequency excitations rather than low frequency. Haslum and Faltinsen (1999) addressed three ways to decrease the wave frequency excitations, including increasing the system damping and heave natural period, and decreasing heave excitation forces.

One of the methods to achieve above goals is to increase the draft. For conventional semis, the typical draft is 20～25 m. By increasing the column draft from 21 m to 40 m, the heave response amplitude operator (RAO) will be reduced by approximately 50% for the period range of interests (Bindingsbø and Bjørset, 2002). However, as the draft increases, prominent vortex-induced motions (VIM) occur (Gonçalves et al., 2012, 2013) and VIM becomes an issue which cannot be neglected in the design.

Another way has been made by installing heave plates. The effectiveness of heave plates on increasing added mass and viscous damping, which result in reducing heave responses consequently, has been proved by many experiments (e.g., Prislin et al., 1998; Thiagarajan and Troesch, 1998; Lake et al., 2000; Thiagarajan et al., 2002; He, 2003; Tao and Dray, 2008) and numerical studies (e.g., Magee et al., 2000; Holmes et al., 2001; Molin, 2001; Tao and Cai, 2004; Tao et al., 2007; Shen et al., 2012). Due to the good

* Corresponding author.
E-mail address: zjiang@shou.edu.cn (Z. Jiang).

http://dx.doi.org/10.1016/j.oceaneng.2016.07.039
0029-8018/

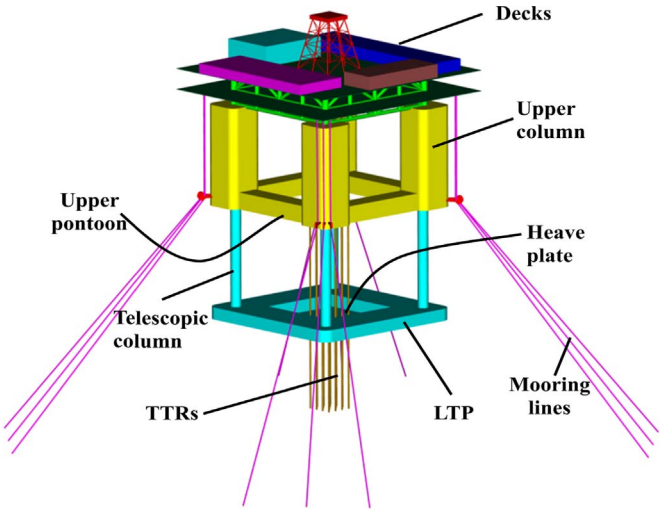

Fig. 1. Deepwater tumbler platform (DTP) rendering (Xie et al., 2012).

recognition of the characteristics of heave plates, they have already been used in the industrial applications of Truss Spar. Recently, many novel dry tree semisubmersible concepts have been developed by utilizing heave plates to improve heave performance so as to satisfy the needs of dry tree systems (e.g., Halkyard et al., 2002; Chakrabarti et al. 2007). However, heave plates can provide little help in improving the stability performance. Besides superior heave performance, better stability is also expected in the development of novel floater concepts (e.g., Murray et al., 2008; Mansour, 2009; Bennett, 2013; Williams et al., 2010).

Deepwater Tumbler Platform (DTP), as shown in Fig. 1, is another solution, which aims not only to be able to support dry tree systems, but also to achieve better stability to suit the environmental conditions in South China Sea (Xie et al., 2012). The hull of DTP concept consists of a conventional semisubmersible hull with lower tier pontoons (LTP) connected by four telescopic columns (TCs). A large heave plate is mounted within the LTP. For the sake of simplicity, the telescopic columns, the heave plate and LTP together are called as telescopic part, and the upper deep draft semisubmersible hull and topsides together are called as main part hereafter.

DTP inherits the advantages of conventional semis, and in addition, DTP utilizes double tier pontoons design to increase added mass, and to reduce the heave responses. Besides, the LTP is installed with high-density solid ballast during operation to adjust the center of buoyancy (COB) above the center of gravity (COG). Consequently, the DTP can keep stable unconditionally like Spars.

However, the effectiveness of using double tier pontoons to reduce heave responses has not been extensively studied in the literature. Furthermore, although the large amount of mass of the LTP together with solid ballast will enable the platform stable, it will also exert big bending moments, horizontal and vertical forces on the connections between TCs and upper columns (UCs), which makes the design of the connection between TCs and UCs another critical issue, which is needed to be addressed.

In such circumstances, this paper will investigate the influence of double tier pontoons on the heave responses and the loads of the critical connections between TCs and UCs in both numerical and experimental methods. The changes of the heave responses and the loads of the critical connection due to varying depths of LTP are also investigated.

2. Description of the DTP systems

2.1. Features of the DTP plans

The DTP studied in this paper is designed to work in the water depth of approximately 1500 m in South China Sea (SCS), to meet the minimum requirements (ABS, 2009) of and to support a 17,657 t topsides weight in the operating condition with seven dry tree risers which are top-tensioned risers (TTRs), and two steel catenary risers (SCRs).

The platform dimensions were derived based on several factors including: restrictions in construction capability, quayside water depth, adequate stability at all phases of operation, small motions, COG and COB positions, and minimized steel weight. An optimization study was carried out to determine the most desirable configuration and dimensions for the DTP. The dimensions of such optimized plan (plan B) are given in Table 1 and a summary of weight distribution is shown in Table 2. To further investigate the influence of LTP elevation below the waterline, two contrast plans were sized by changing TC length ± 5 m, named plan A and plan C respectively. Consequently, the LTP elevation (i.e. draft), total length and loading conditions of plan A and plan C are different from plan B, as shown in Table 3 and Fig. 2. Other main dimensions remain unchanged.

All of the plans adopt the same mooring system, which includes twelve mooring lines arranged in four groups, as shown in Fig. 3. The four groups are arranged symmetrically about the centerline of the DTP. Each mooring line consists of a platform chain at the top, a polyester rope in the middle, a pile chain at the bottom and connectors between the rope and the chains. Total pretension of each line is 2225 kN. Table 4 shows the mooring line properties.

2.2. Description of the critical connection

A design premise for DTP is that it needs to be towed to the deepwater reservoir location as a whole in the upright position. Therefore, the upper columns and telescopic columns could not be welded together in the shipyard and need to be connected offshore. The structural reliability of such connections, which are performed offshore, requires more attentions. Furthermore, according to the predictions of sectional loads at various elevations along the DTP hull, the maximum bending moments happen at the elevation of the connection between TCs and UCs (Jiang et al., 2012). Consequently, the structural design of such connection becomes one of the most critical aspects of DTP. Two main issues should be considered, i.e. the selection of connection methods and an accurate estimate of design loads for the connection structures. In fact, the level of loads has much impact on the selection of connection methods. So this paper will focus on the estimation of

Table 1
Main particulars of plan B.

Parameter	Unit	Value
Upper column size (Length × Width × Height)	m × m × m	20.6 × 20.6 × 47.0
Upper column center spacing	m	60.6
Upper pontoon size (Length × Width × Height)	m × m × m	81.2 × 15.0 × 8.6
LTP size (Length × Width × Height)	m × m × m	81.2 × 20.6 × 2.0
TC diameter	m	5.4
TC length	m	46
Heave plate	m × m	40.0 × 40.0
Draft	m	80.0
Displacement	ton	90,930
Displacement of main part	ton	76,381
Displacement of telescopic part	ton	14,549
Center of buoyancy from keel	m	52.3

Table 2
Summary of weight distribution.

Parameter	Unit	Value
Main part weight	MT	46,550
Telescopic part weight	MT	35,040
Mooring vertical load	MT	4540
TTR and SCR payload	MT	4800
Center of gravity from keel	m	50.5

Table 3
Main dimensions of the three plans.

	Plan A	Plan B	Plan C
TC length (m)	51	46	41
LTP depth (m)	85.0	80.0	75.0
Displacement (ton)	91,400	90,930	90,461
COG (m)	54.2	52.3	46.5

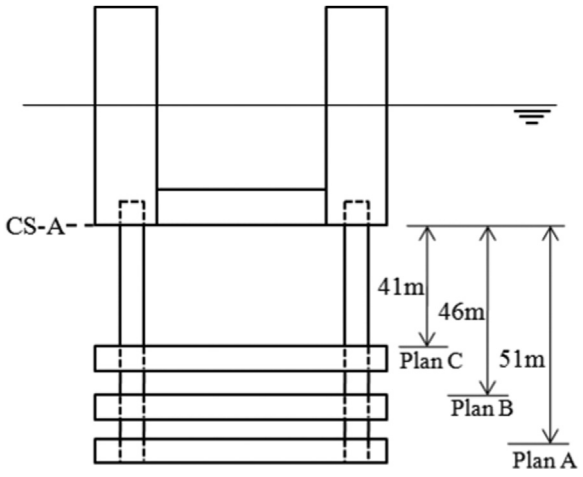

Fig.2. Definitions of Plan A, Plan B, Plan C and cross sections A.

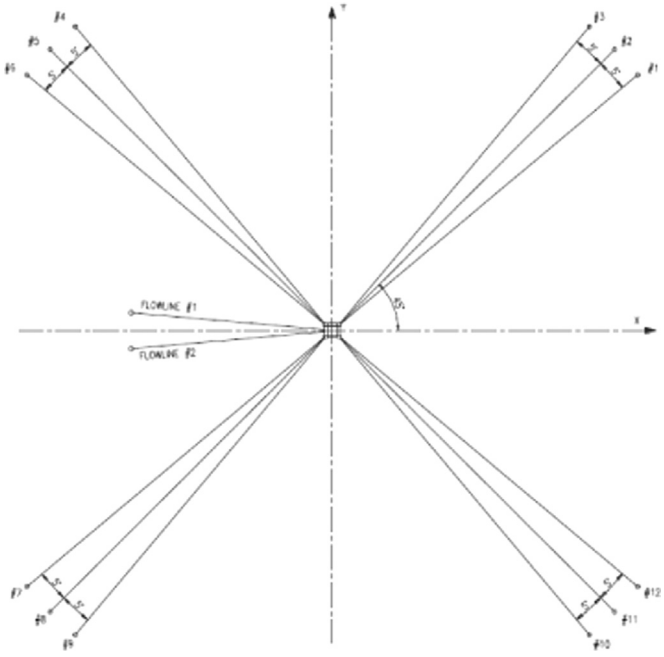

Fig.3. The arrangement of mooring lines.

Table 4
Mooring line properties.

Segment	Anchor chain	Polyester rope	Platform chain
Segment grade	R4S	Polyester	R4S
Nominal diameter (m)	0.13	0.257	0.13
Length (m)	300	1900	175
Wet weight (kg/m)	293	10.6	293
Minimum breaking load (kN)	17,262	17,858	17,262
Axial stiffness (N)	1.3E9	2.3E8	1.3E9

Table 5
Parameters of the environmental conditions.

No.	Wave			Wind	Current
	Significant height (m)	Peak period (s)	Peak enhancement factor	Velocity (m/s)	Velocity at surface (m/s)
SS.1	7.0	12.1	2.0	/	/
SS.2	13.8	16.1	2.4	/	/
SS.3	13.8	16.1	2.4	40.9	2.02

the design loads of connection between TCs and UCs.

The global vertical, horizontal and rotational loads of the connections were calculated in both numerical simulation and model tests. To be more specific, the sectional loads at the elevation of cross section A (CS-A, shown in Fig. 2) were analyzed and discussed hereafter as a representation of the connection loads.

2.3. Environmental conditions

The design environmental conditions in South China Sea are listed in Table 5. The random wave components are described by a three-parameter JONSWAP spectrum for 1 year (1-yr) and 100 year (100-yr) waves respectively.

Three sea states combinations are studied in both the numerical computations and model tests. For 1-yr sea state (SS.1), only 1 yr wave is considered, without wind or current. For 100-yr sea state, two sea states are considered, one with 100-yr wave only (SS.2) and the other with 100-yr wind, wave and current combined (SS.3). The wind, wave and current are assumed to be co-linear in SS.3.

Note that, for an engineering design, more sea states should be studied including 1000-yr survival conditions, 1 yr wind, wave and current combined condition, and non-collinear environmental conditions, etc.

3. Numerical simulation method and model test

3.1. Numerical simulation

Both frequency domain analysis and non-linear time domain analysis have been conducted to determine the global responses of the platform and to verify the mooring system design. Only frequency domain analysis was used to obtain the local sectional loads for the connections.

The frequency domain analysis was conducted using the SESAM Hydro.D (DNV, 2014). This is a hydrodynamic analysis program that calculates motions based on a constant panel method radiation/diffraction code. Newman's approximation is used to calculate 2nd order wave force (Newman, 1974), which is also integrated in the software. Viscous contributions to wave forces and damping are estimated using Morison formulation members. The drag coefficients used in this study are listed in Table 6. Note

Table 6
Drag coefficients used in this study.

Component	Direction	Value
Upper columns	Lateral	1.05
	Axial	0.85
Upper pontoons	Lateral	1.20
	Axial	1.00
LTPs	Lateral	1.20
	Axial	1.00
Telescopic columns	Axial	0.90
Heave plates	Axial	4.00

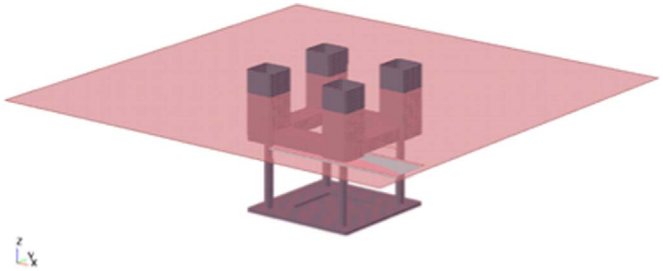

Fig. 4. DTP hull panel model.

that these data needs to be further verified when more experimental results are obtained. The DTP hull was modeled as panels as shown in Fig. 4.

The hull/mooring coupled analysis in time domain was conducted using SESAM SIMO/RIFLEX program (Marintek, 2014a, 2014b). Colby et al. (2000) and Hansen et al. (2004) defined the coupling effects as the influence on floater mean position and dynamic response from slender structure restoring, damping and inertia forces. It is hard to include a complete description of the numerical simulation method in the short space of this article. Briefly, in the coupled approach mentioned here, the total loads (dynamics included) from the "slender body models" of mooring lines are transferred as a force into the "large body" model of the floater. Irregular wave frequency (WF) and low frequency (LF) environmental loading is required to give an adequate representation of the dynamic behavior of the coupled vessel/slender structures system. Dynamic equilibrium between the forces acting on the floater and slender structure response is satisfied at every time instant and thus the assessment of the low frequency damping from the slender structure is not needed.

$$R^I(r, \ddot{r}, t) + R^D(r, \dot{r}, t) + R^S(r, t) = R^E(r, \dot{r}, t) \quad (1)$$

where R^I, R^D and R^S represent the inertia, damping and internal reaction force vectors respectively, R^E is the external load vector, r, $\dot{r}$ and $\ddot{r}$ are the structural displacement, velocity and acceleration vectors respectively.

The inertia force vector is expressed as

$$R^I(r, \ddot{r}, t) = M(r)\ddot{r} \quad (2)$$

where M is the system mass matrix that includes structural mass and hydrodynamic mass. The damping force vector is expressed as

$$R^D(r, \dot{r}, t) = C(r)\dot{r} \quad (3)$$

where C is the system damping matrix.

The internal reaction force vector $R^S(r, t)$ is calculated based on the instantaneous state of stress. The external load vector

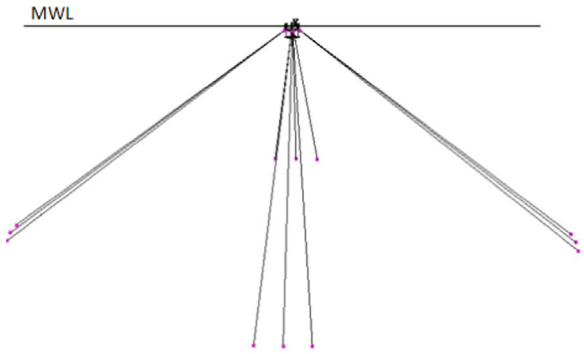

Fig. 5. Coupled analysis model.

$R^E(r, \dot{r}, t)$ accounts for the weight and buoyancy, forced displacements, environmental forces and specific forces.

The finite element model of mooring lines consists of bar elements only, i.e., bending stiffness and torsion stiffness are neglected. Hydrodynamic forces are modeled by means of the generalized Morison equation. Both TTRs and SCRs were modeled as fixed masses, which was the same with what were simulated in the model test. Coupled analysis model for the DTP and mooring system is shown in Fig. 5.

3.2. Model test

Model tests were conducted in the wave basin in the State Key Laboratory of Ocean Engineering located in Shanghai Jiaotong University. The results of the model tests were used to verify the numerical results. The wave basin is 50 m long, 40 m wide and 10 m deep. A scale ratio of 1:60 was selected, shown in Fig. 6.

A constant wind field was formed up around the model to simulate the design wind as shown in Table 5. Due to the limitation of the wind simulation capability, wind dynamic effects could not be modeled in the tests, which may have some influence in the hydrodynamic characteristics, especially in the horizontal plane. The simulated Jonswap spectrum in the model tests and the theoretical wave spectrums for 1-yr and 100-yr waves were exhibited in Fig. 7a and b respectively. The current generation system was used to simulate the design current profile, shown in Fig. 8. The current profile was measured using Doppler velocimetry at the center of the model and the current turbulence level in the basin is less than 10% on the root mean square (RMS). The current profile was measured before the DTP model was placed. The definition of the coordinates in the model tests is shown in Fig. 9.

Free decay tests, regular wave tests and irregular wave tests were performed for plan A, plan B and plan C. Besides obtaining hydrodynamic characteristics of DTP, the sectional loads at CS-A were captured as well. A special device tailored to this study was adopted, as shown in Fig. 10. For each connection, one 6-component-force sensor was used to connect the upper column and the telescopic column through aluminum plates on both sides, which could also serve as reinforcement structures, shown in Fig. 10. The stiffness of such combined structures could be regarded as fixed joints. In all of the test cases, wind, current and wave are coming from single direction (0°). Other headings could be more critical for some characteristics. Since heave performance is what we cared most in this study and direction of environmental loads does not play a big role in the heave performance. Hence, only 0° is considered.

Three signal channels of the pre-calibrated sensors were used, i.e. *Fx*, *Fz* and *My*. The measurements of the sensors represent the loads of each connection, while only total sectional loads can be obtained through the numerical analysis. For the sake of comparison, the total sectional loads at CS-A can be expressed as

Fig. 6. Physical model of DTP.

$$Fx.\ T = \sum_{1}^{4} Fx_i \tag{4}$$

$$Fz.\ T = \sum_{1}^{4} Fz_i \tag{5}$$

$$M_y.\ T_i = M_{yi} + (F_{z3} + F_{z4} - F_{z1} - F_{z2})*L \quad for\ i = 1, 2 \tag{6}$$

$$M_y.\ T_i = M_{yi} + (F_{z1} + F_{z2} - F_{z3} - F_{z4})*L \quad for\ i = 3, 4 \tag{7}$$

As shown in Fig.11, i denotes the number of the connection; L is the telescopic column center spacing (i.e. the upper column center spacing); $Fx.\ T$ is the total force at section CS-A in horizontal direction; $Fz.\ T$ is the total force at section CS-A in vertical direction; $M_y.\ T_1$ and $M_y.\ T_2$ are the total bending moments about Y axis at section YZ-1; $M_y.\ T_3$ and $M_y.\ T_4$ are the total bending moments of section YZ-2.

Due to the limit of sensors' range, the static part of load due to the gravity load and buoyancy was pre-balanced during calibrating. Only the inertia force and dynamic force were measured in the model tests, which were defined the same with the values obtained in the numerical analysis.

All the equipment and sensors have been calibrated before tests.

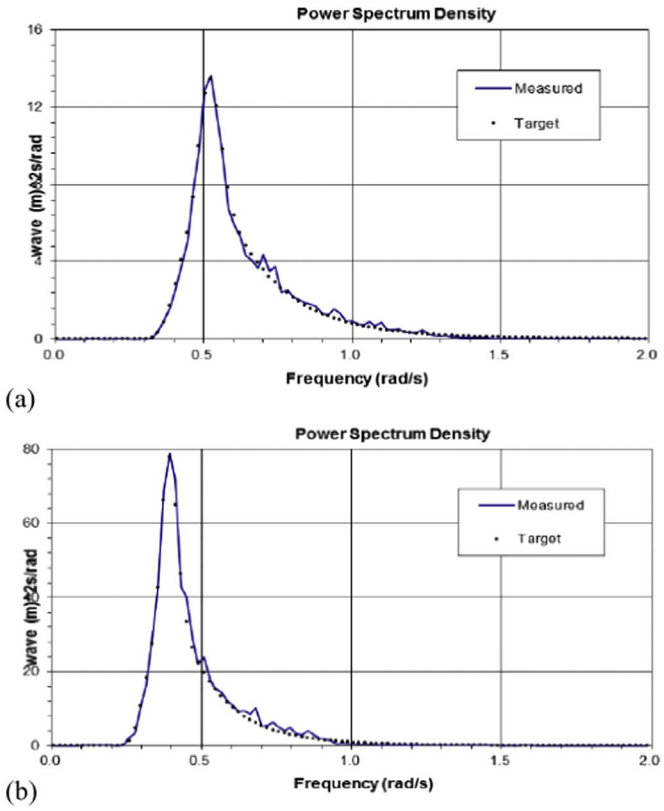

Fig. 7. Comparison of the theoretical wave elevation spectral density and the measured one. (a) 1-yr wave, (b) 100-yr wave.

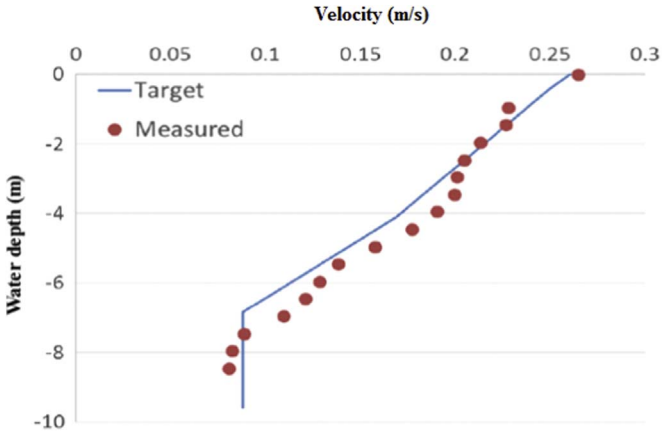

Fig. 8. Comparison of the design current profile and the measured one in scaled values.

4. Results and discussions

4.1. Free decay test results

The natural periods and damping coefficients for roll, pitch and heave responses were obtained through free decay tests in the wave basin, shown in Fig. 12. The natural periods were computed by average of 10 consecutive period cycles of the free decay test. The damping coefficients were calculated by the ratio between two consecutive wave amplitudes of wave crests or troughs obtained through the single degree free decay test. The results for the three plans are shown in Table 7. From Table 7, it can be seen that the heave natural periods for all the plans are above 30 s, which is much larger than that of a conventional semisubmersible due to extra added mass introduced by LTP. The heave natural periods of

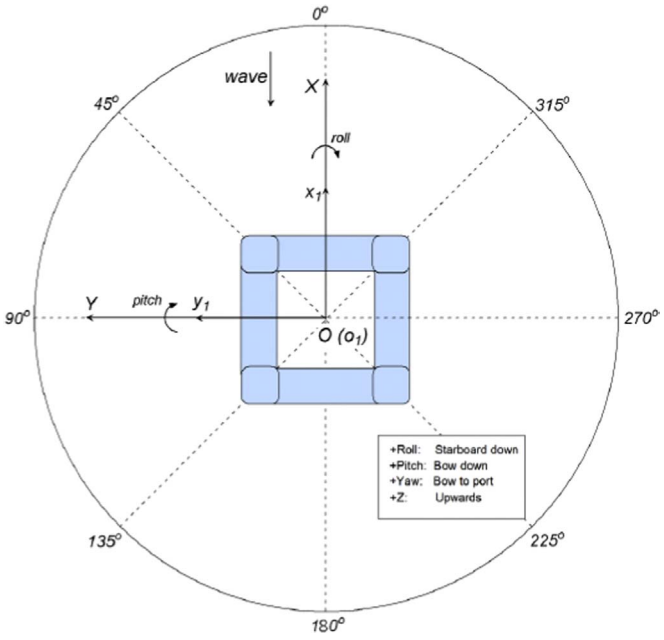

Fig. 9. Coordinates definition in the model tests.

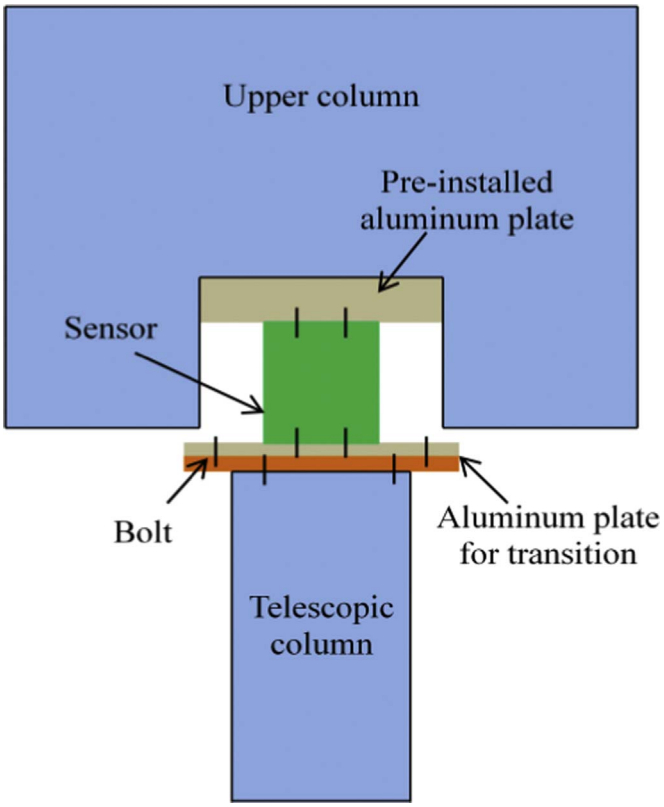

Fig. 10. Sensor installation used for model test.

the three plans are away from the normal wave energy concentration zone. The motions' natural periods with (w/) or without (w/o) the mooring system for the three plans in the model tests are also listed in Table 8.

Free decay tests were also performed in the numerical analysis for plan B, shown in Table 9. From Table 9, it can be observed that both numerical and experimental methods yield similar results, except for some minor differences in the values.

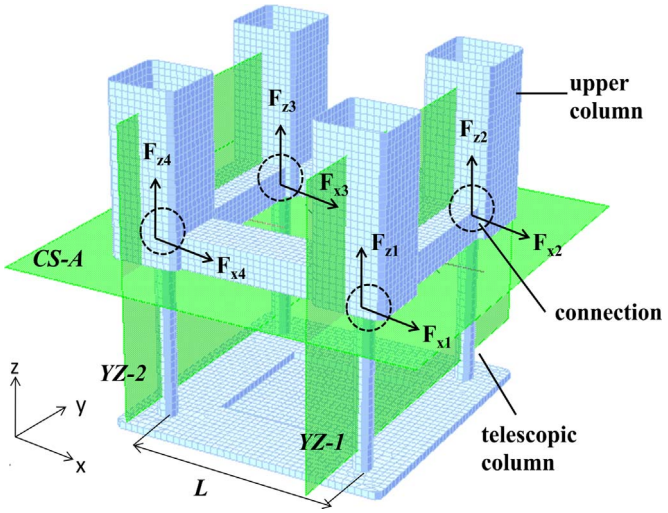

Fig. 11. Definition of loads measured by the sensors.

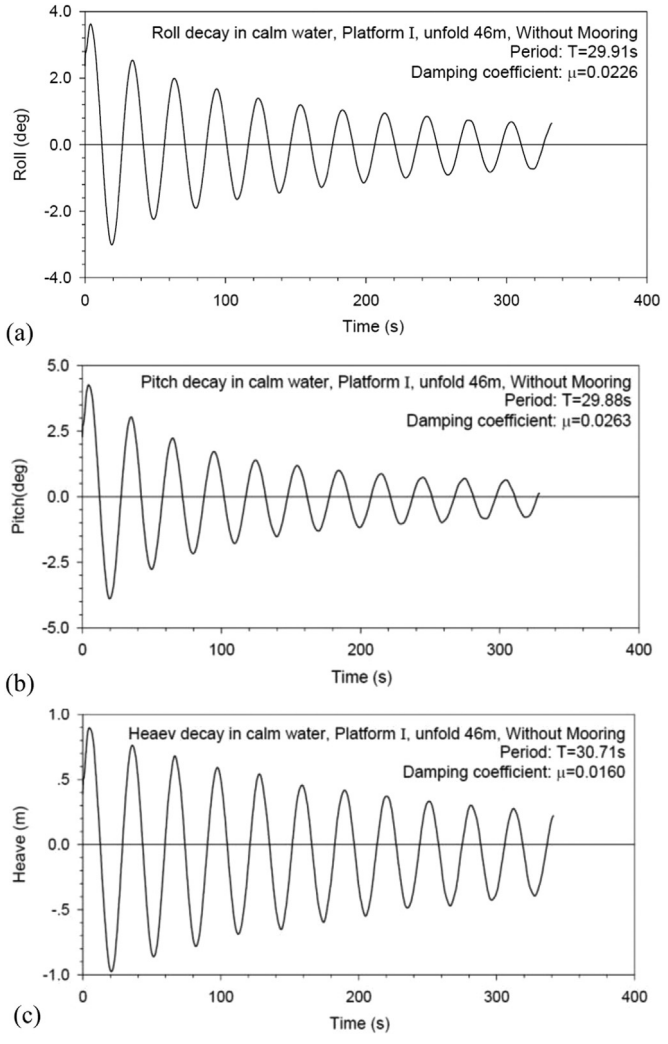

Fig. 12. Free decay curves for plan B in the free floating condition: (a) roll decay curve, (b) pitch decay curve, and (c) heave decay curve.

4.2. *Response amplitude operators (RAOs)*

Among all six-degree-freedom motions, the RAOs of the vertical (heave), lateral (surge) and rotational (pitch) motions are

Table 7
Natural periods and damping coefficients.

		Plan A	Plan B	Plan C
Natural period (s)	Roll	31.4	29.9	29.9
	Pitch	31.3	29.9	29.7
	Heave	30.8	30.7	30.6
Damping coefficient	Roll	0.026	0.023	0.023
	Pitch	0.024	0.026	0.027
	Heave	0.019	0.016	0.019

Table 8
Natural periods with (w/) or without (w/o) the mooring system for the three plans in the model tests.

			Plan A	Plan B	Plan C
Period (s)	Roll	W/o mooring	31.4	29.9	29.9
		W/ mooring	29.0	27.6	27.6
	Pitch	W/o mooring	31.3	29.9	29.7
		W/ mooring	29.0	28.0	27.6
	Heave	W/o mooring	30.8	30.7	30.6
		W/ mooring	30.3	30.06	30.0

Table 9
Comparison of natural periods for plan B between numerical and experimental methods.

Natural period (s)	Roll	Pitch	Heave
Model test	29.9	29.9	30.7
Computation	28.5	28.5	31.5

mainly discussed by both frequency domain analysis and regular wave tests. Because of the large natural period of heave indicated from free decay test results, the wave periods were taken from 4 s to 37 s both in the numerical simulation and model tests.

4.2.1. Numerical and experimental results for plan B

The comparisons of heave, pitch and surge RAOs for plan B between numerical analyses and model tests are plotted in Figs. 13–15. The periods are displayed along the *x* axis and are converted to the prototype scale. It can be seen that the RAOs obtained from numerical analyses present similar trends with those of the model tests for the three motions. In addition, the RAO amplitudes from numerical analysis match well with those of the model tests for periods less than 25 s. For longer wave periods, say greater than 25 s, the agreement becomes poorer. When simulating the waves with periods greater than 25, the wave energy is quite low, which may be attributed to the inaccuracy of results. For the heave behavior, both methods present double peaks, with the first peak at around 22 s and the amplitude of 0.3. However, the RAO curve from numerical analysis drops down much more dramatically than that of the model tests and it approaches to nearly zero at the "cancellation period", which is commonly found in numerical analysis for semis. Note that no "cancellation period" was observed in the model tests. Overall, the heave motions are small in the main wave energy zone.

To have a further study on the heave RAO of DTP, a conventional semi and a truss Spar were analyzed numerically for comparison. The selected conventional semi and Spar are of the same deck load capacity as plan B. The RAO results are also depicted in Fig.13. From Fig. 13, DTP shares the same characteristics as the

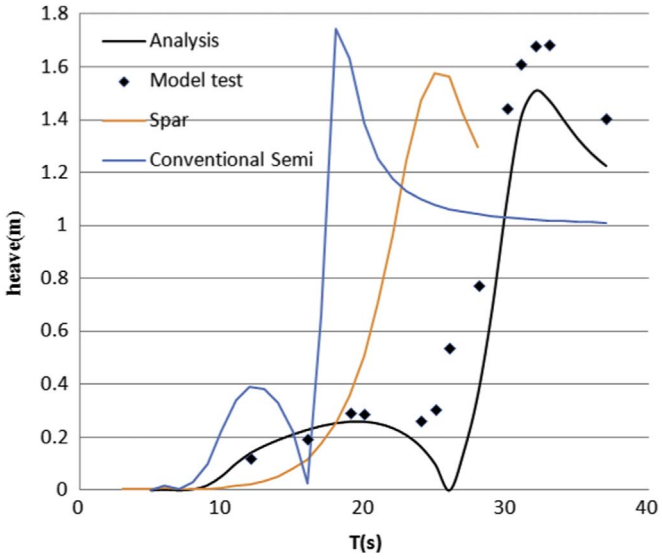

Fig.13. Heave RAO comparison among numerical analysis, model tests of plan B, a Spar and a conventional semi.

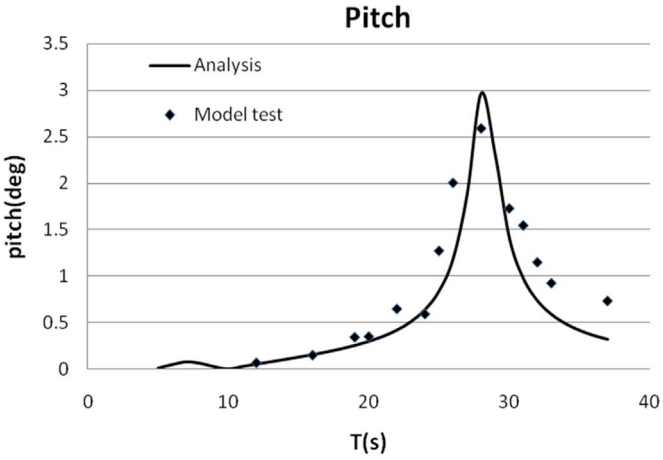

Fig.14. Pitch RAO comparison between numerical analysis and model tests of plan B.

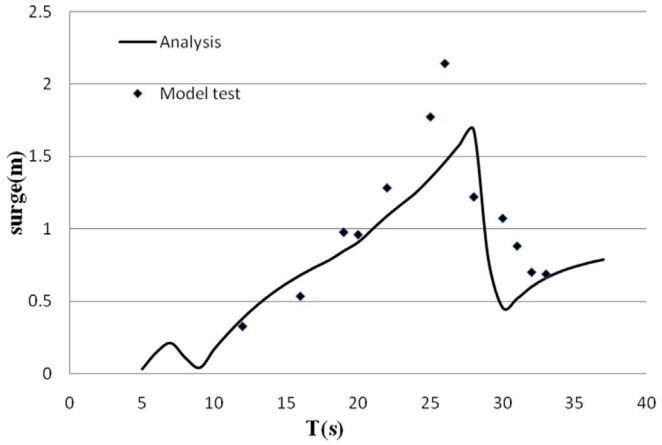

Fig.15. Surge RAO comparison between numerical analysis and model tests of plan B.

conventional semi that both have double peaks, but the first peak of DTP is much smaller than that of a conventional semi. In addition, the heave natural period of DTP is further shifted away

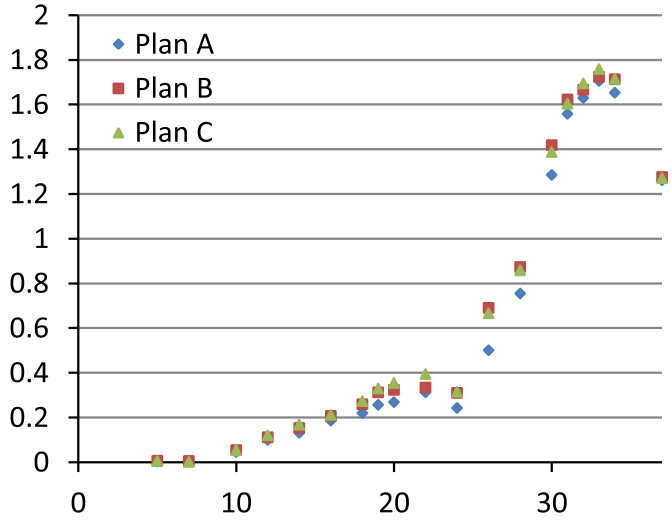

Fig.16. Heave RAOs for the three plans obtained in the model tests.

from the peak wave period contrasting to a conventional semi. For the comparison between plan B and the Spar, these two concepts show different heave characteristics. The heave amplitudes of the Spar are much smaller than those of plan B for the periods before around 18 s, while the contrary when the periods are greater than 18 s.

4.2.2. Experimental results comparison for the three plans

Similar regular wave tests were conducted for plan A and plan C as well. Table 9 displays the peak values with corresponding periods of heave RAOs for all the plans. The heave RAOs comparison is shown in Fig. 16. From Table 10 and Fig. 16, it can be seen that both 1st peak and 2nd peak happen at the same periods for all three plans and as the draft increases, the peak values decreases for both 1st and 2nd peak, which indicates that the elevation of LTP affects the amplitudes of heave performance.

4.3. Motions and mooring loads

4.3.1. Numerical and experimental results for plan B

The time-domain non-linear analyses and model tests were conducted for plan B under the three sea states listed in Table 5. In the time domain analyses, each simulation is performed for three-hour duration in a single realization. More random wave seeds need to be analyzed and statistical analysis should be conducted to provide stable values in the future. The maximum motions and mooring loads of DTP were attained as shown in Table 11.

The maximal surge motions are 68.6 m and 75.3 m in SS.3 in the model tests and numerical analysis respectively. The mean surge motions are 39.6 m and 40.5 m in SS.3 in the model tests and numerical analysis respectively. The maximal heave motions (single amplitudes), occurring in SS.3, are 3.6 m and 3.8 m in the model tests and numerical analysis respectively, which once again demonstrates that the DTP has much better heave performance comparing with conventional semis. The maximum heave amplitudes are at the same level with typical heave performance of

Table 10
Peak values with corresponding periods of heave RAOs for all the plans (with mooring).

	Plan A	Plan B	Plan C
1st peak value(m/m) @resonance period(s)	0.31@22	0.33@22	0.39@22
2nd peak value(m/m) @resonance period(s)	1.70@33	1.72@33	1.76@33

Table 11
Motion and mooring load statistics comparison between model tests and numerical analysis for plan B.

Sea States	Parameter	Model test	Numerical simulation	Difference
SS.1	$\|Heave\|_{max}$ (m)	1.0	0.9	10.0%
	$\|Heave\|_{sd}$ (m)	0.25	0.23	8.0%
	$\|Pitch\|_{max}$ (deg)	1.4	1.0	28.6%
	$\|Pitch\|_{sd}$ (deg)	0.33	0.29	12.1%
SS.2	$\|Heave\|_{max}$ (m)	3.8	4.1	7.9%
	$\|Heave\|_{sd}$ (m)	0.77	0.81	5.2%
	$\|Pitch\|_{max}$ (deg)	4.4	5.9	34.1%
	$\|Pitch\|_{sd}$ (deg)	1.0	1.1	10.0%
SS.3	$\|Heave\|_{max}$ (m)	3.6	3.8	5.6%
	$\|Heave\|_{sd}$ (m)	0.73	0.75	2.7%
	$\|Pitch\|_{max}$ (deg)	5.2	6.2	19.2%
	$\|Pitch\|_{sd}$ (deg)	0.88	0.94	6.8%
	$\|Surge\|_{max}$ (m)	68.6	75.3	9.8%
	$\|Surge\|_{sd}$ (m)	5.6	6.0	7.1%
	$Fline_{max}$ (ton)	799.6	830.8	5.0%
	$Fline_{sd}$ (ton)	34.9	36.0	3.2%

Spars. Note that the maximum heave motion in SS.2 is larger than that of SS.3. When encountering the wind and current force as defined in SS.3, the platform starts to drift away and the semi-taut mooring lines not only functions to restrain the horizontal offset, also provides additional vertical stiffness, consequently, heave motions are constrained to a certain extent. The effect of vertical stiffness by mooring lines plays an even bigger role in model tests due to the truncation technique used in model tests. It needs further attention in the DTP design. The comparison of heave motions between SS.2 and SS.3 also demonstrates that the wave induced excitation takes a majority part of the total heave excitation force. The model test results of the heave, surge and pitch motions in the time history are shown in Fig. 17–19.

The maximum mooring tension is 799.6 t and 839.8 t in SS.3 in the model tests and numerical analysis respectively, which are below the line breaking strength with a safety factor of 1.67. Fig. 20 shows the mooring tension time history for line 1 in the model test, where the maximum mooring tension happened. The heave response spectrums of SS.2 and SS.3 are analyzed by Fast Fourier Transformation as shown in Fig. 21. From Fig.21, it could also been found that the heave motion is more governed by wave frequency force.

The mooring loads of plan B are well below the design criteria. It could also be seen from Table 10 that the results by numerical simulation match well with the results of model tests, except the maximal pitch motion in SS.2. The maximum value is a single peak in a single numerical realization, which is of more randomness

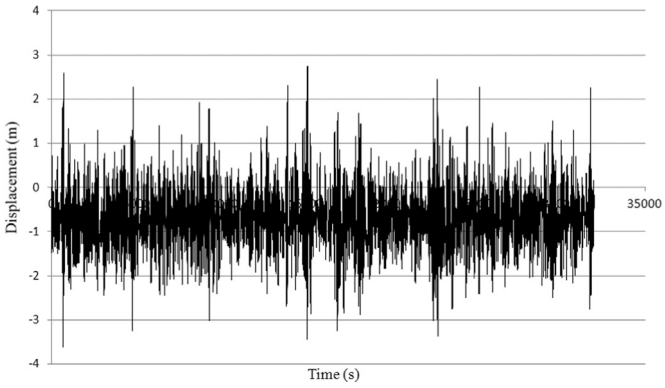

Fig. 17. Heave time history for plan B in SS.3 in the model test.

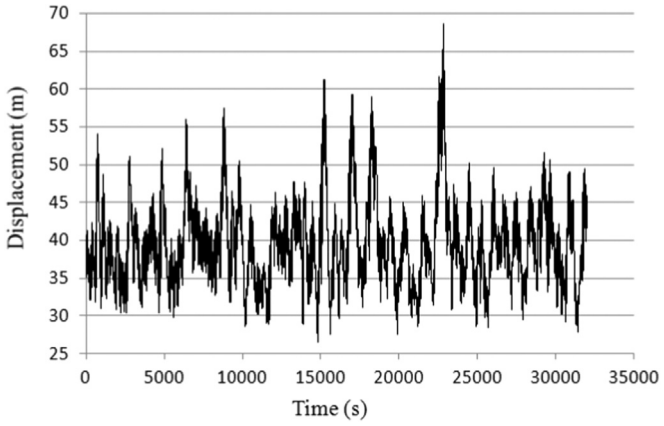

Fig. 18. Surge time history for plan B in SS.3 in the model test.

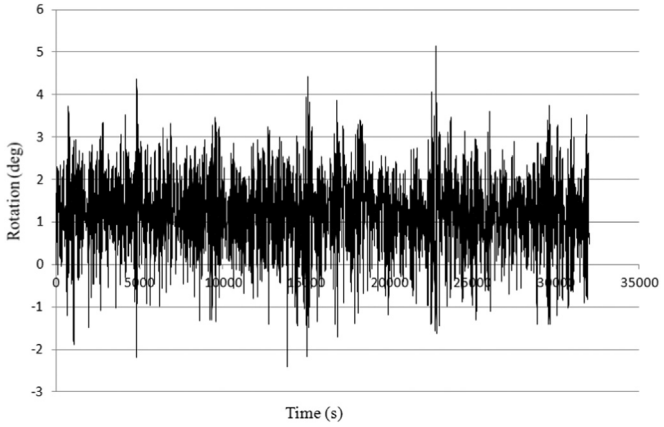

Fig. 19. Pitch time history for plan B in SS.3 in the model test.

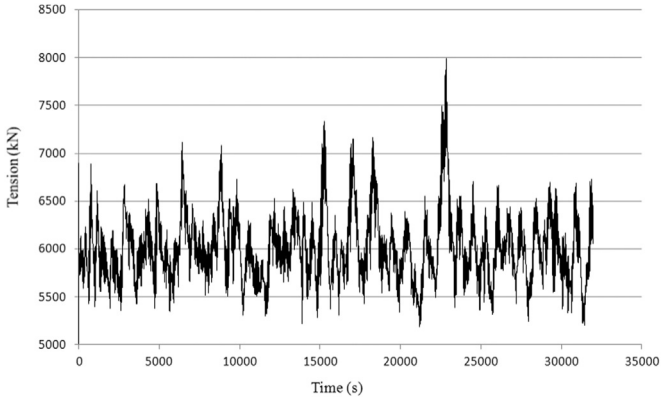

Fig. 20. Mooring tension time history for plan B in SS.3 in the model test.

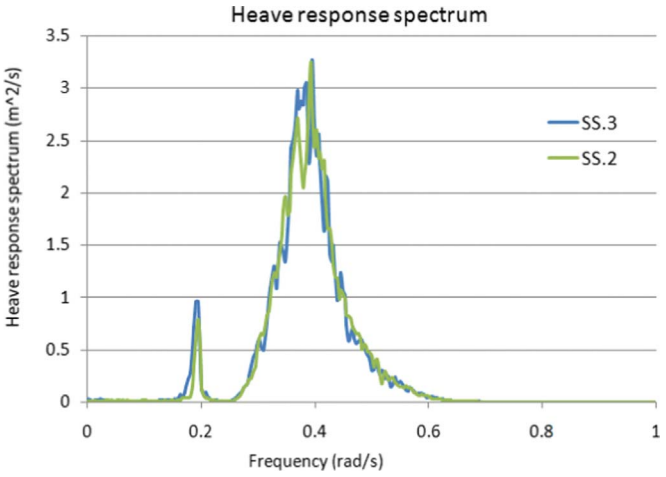

Fig. 21. Heave response spectrum comparison between SS.2 and SS.3.

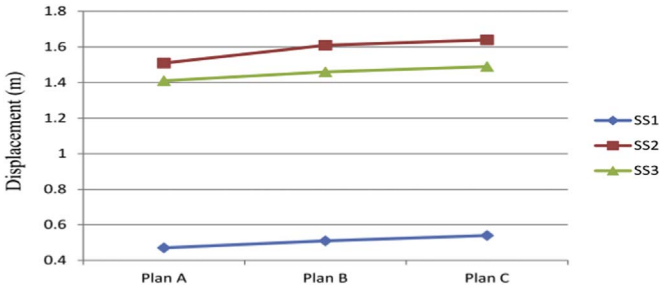

Fig.22. Comparisons of $|H_{1/3}|$ for the three plans in SS.1～SS.3.

than significant values. By comparing the standard deviation values shown in Table 11, it could be found that the numerical results match the model test results well.

4.3.2. *Experimental results comparison for the three plans*

In this section, the heave motions obtained in the model tests for the three plans were discussed. A statistical analysis was made to analyze the average of top one-third of heave amplitudes ($|H_{1/3}|$). Comparisons of $|H_{1/3}|$ for the three plans in SS.1～SS.3 are shown in Fig.22. The three lines in the figure exhibit similar trends that when the elevation of LTP below the waterline decreases, the heave responses increases. Such trends indicate that the effect of double tier pontoons becomes bigger when the LTP is located in a deeper elevation. In this study, the change of heave responses is not quite prominent with the largest change ratio at 8.5%. This is attributed to the small change of LTP depth among the three plans, for the sake of maintaining the rationality of plan A and plan C. However, it could be easily deducted that if larger differences of LTP elevation among the three plans are chosen, larger changes of heave motions will be found. There is of course maximum design limit on the LTP elevation. Firstly, the sectional loads increase as the LTP elevation increase. And to some extent, it would be very hard to conduct the structural design for the connections between upper columns and telescopic columns. Secondly, when reaching certain depth, the effect of lowing heave plates on reducing heave response is getting smaller. From both the numerical and experimental results of heave motions and the heave RAOs discussed above, the effectiveness of double tier pontoons can be proved.

Besides, for plan A and plan C, the heave motions in SS.3 are smaller than those in SS.2 as well, as it has been explained above for plan B.

4.4. *Connection loads*

4.4.1. *Numerical and experimental results for plan B*

As mentioned in Section 3.1, the low frequency force was not accounted in calculating sectional loads due to the software limitation, so the comparison for SS.3, in which the low frequency force may take a large part, may not be meaningful and therefore will not be presented here. The sectional loads in the wave only conditions (i.e. SS.1 and SS.2) in the model tests were obtained using the sensor equipment and further compared with numerical analysis results in the frequency domain.

The RAOs of sectional forces and bending moments at CS-A are as shown in Figs. 23–25. The peaks of the RAOs of F_z and M_y are about 30 s, which coincide with the natural periods of heave shown in Fig. 12. With the short term predictions, the maximum

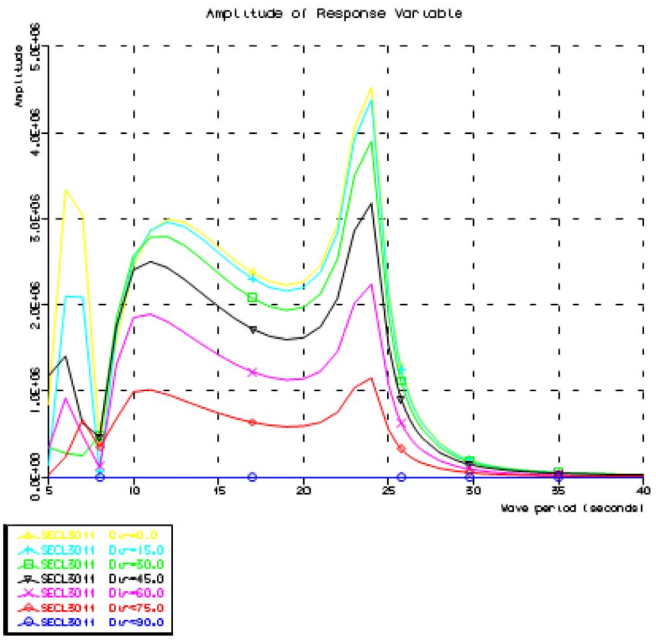

Fig.23. The RAO of *Fx* by numerical analysis of plan B.

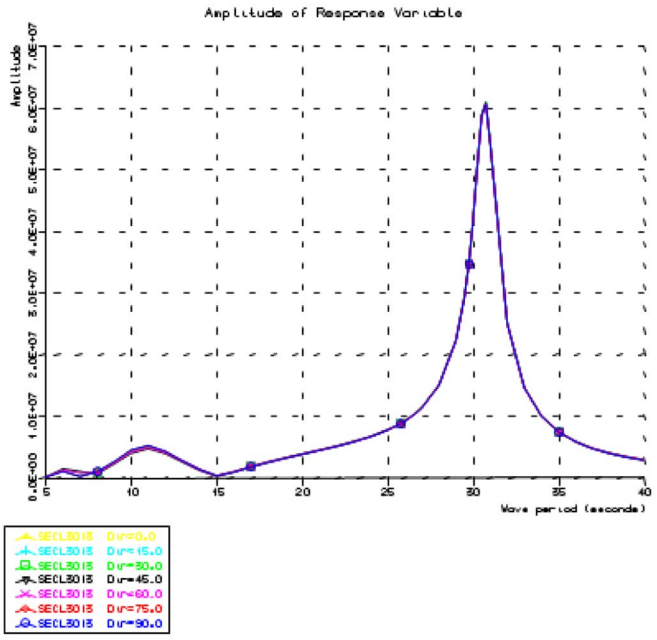

Fig.24. The RAO of *Fz* by numerical analysis of plan B.

sectional forces and bending moments were computed on the basis of Rayleigh distribution for a probability of exceedance of 0.001. Also it should be mentioned that the low frequency wave force is not taken into account in the numerical analysis of sectional loads, which may introduce some differences between numerical analysis and model tests.

Both numerical and experimental results showed that the use of LTP brings in large loads. Table 12 presents comparisons of the maximum vertical force and bending moment between the numerical analyses and model tests for plan B. It can be seen that the results of numerical computations are at the same order of magnitude with the model test results. Besides, the differences of both maximum *Fz.T* and *My.*T values in 1-yr sea state are smaller than those of 100-yr sea state. The differences of maximal *Fz.T* values in both 1-yr and 100-yr sea states are smaller than those of

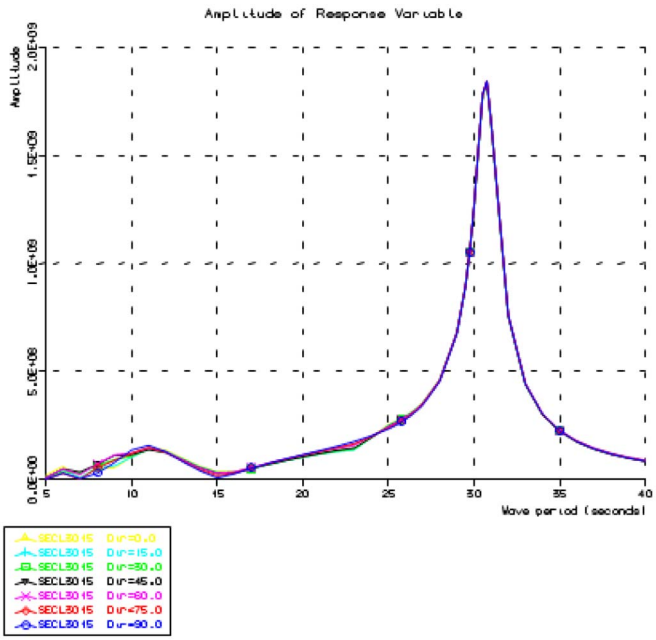

Fig.25. The RAO of *My* by numerical analysis of plan B.

Table 12
Comparisons of the maximum vertical force and bending moment between model tests and numerical analysis for plan B.

Sea States	Parameter	Model test	Numerical simulation	Difference
SS.1	*Max. Fz.T* (kN)	2.35E4	2.28E4	3.0%
	Max. My.T (kN*m)	5.28E5	4.60E5	12.9%
SS.2	*Max. Fz.T* (kN)	4.24E4	3.41E4	19.6%
	*Max. My.*T (kN*m)	1.65E6	1.24E6	24.8%

maximum *My.*T. The results of sectional loads at CS-A provide references in local structural design and also help in the selection of connection methods between UCs and TCs.

4.4.2. *Experimental RESULTS COMPARISON FOR THE THReE plans*

In this section, the forces and bending moments measured in the model tests for the three plans were discussed. The significant values of $F_x.T$, $F_z.T$ and $M_y.T$ were statistically analyzed and compared among the three plans in SS.1～SS.3. The significant values (i.e. $F_x.T_{1/3}$, $F_z.T_{1/3}$, $M_y.T_{1/3}$) here are defined as the mean value of the largest third of the forces or bending moments. The absolute significant values for the forces are shown in Fig. 26(a)–(b). The significant values of the bending moments for each connection are statistically analyzed separately and the maximum among the four connections, $|M_y.T_{1/3}|_{max}$, is shown in Fig. 26(c). These plots present a consistent trend that as the LTP elevation below the waterline increases, the vertical force, horizontal shear force and bending moment at CS-A increases simultaneously. The changes for bending moments among the three plans are much larger than those of vertical and horizontal forces.

To obtain more accurate load results of the connection areas, a detailed structural design should be conducted in advance to simulate the real stiffness of the structure and it would be better to conduct a local structural or mechanical test when the connection methods are determined. It should be pointed out as well that the low frequency force has also impact on the local loads, especially for the horizontal force. These issues will be studied in the future.

To sum up, as the elevation of the LTP below the waterline increases, the heave amplitude decreases while the sectional loads

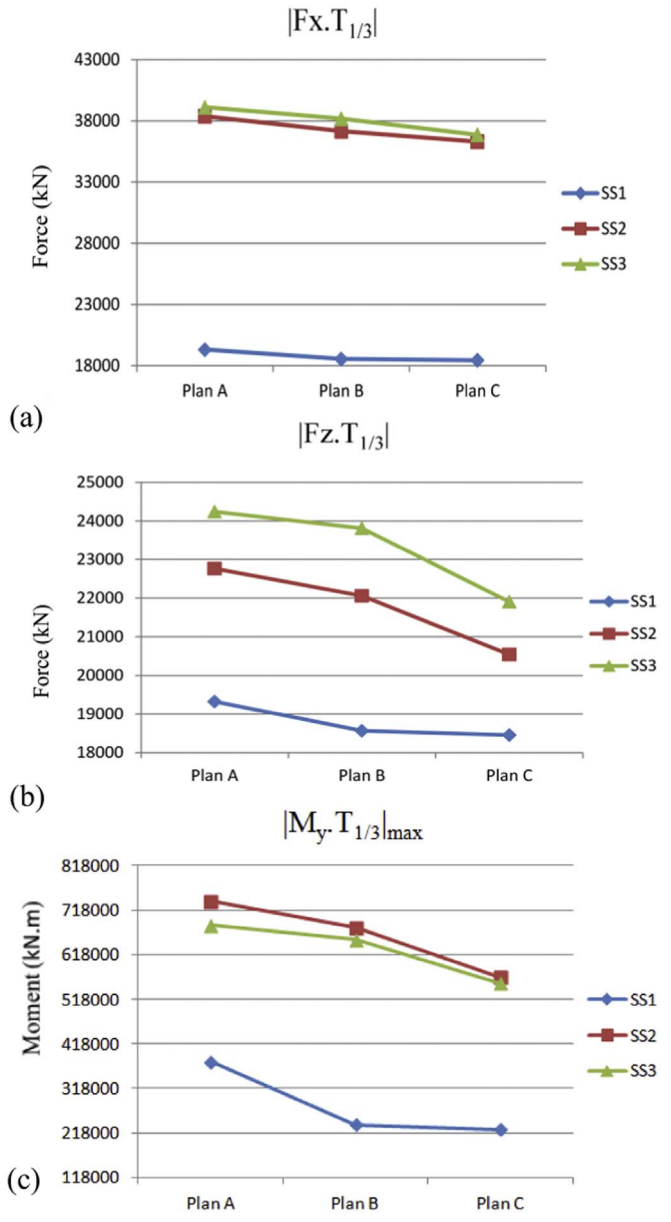

Fig. 26. Statistical results for the three plans in SS.1 ~ SS.3. (a) $|F_x.T_{1/3}|$; (b) $|F_z.T_{1/3}|$; (c) $|M_y.T_{1/3}|_{max}$;.

increase. From the mathematical point of view, an optimization of the LTP elevation should be conducted considering the trade-off between connection loads and heave responses. However, from the engineering point of view, as the connection between telescopic columns and upper columns need to be done offshore by welding, grouting or mechanical methods, such connection would become a vital design issue no matter what kind of methods taken. So normally a designer will expect to have the least local connection loads to ensure the structural safety. In such circumstances, an optimized solution in practical engineering should be found as the minimal LTP elevation that could qualify the requirements of supporting dry tree systems.

5. Summary and conclusions

Deepwater Tumbler Platform (DTP) is a newly proposed concept in the offshore industry, where the design of double tier pontoons is utilized to achieve better heave performance comparing with conventional semisubmersibles.

In the present study, the hydrodynamic performance of DTP and the loads of critical connections have been numerically and experimentally studied. A sensitivity study of the depth of lower tier pontoons (LTP) has also been conducted. Following conclusions can be drawn from the study.

(1) The effectiveness of double tier pontoons on improving hydrodynamic performance, the heave motion particularly, can be observed from both the numerical analyses and model test results. The DTP concept presents a large natural period and relatively low extreme motions in heave comparing with conventional semisubmersibles.
(2) By increasing the elevation of LTP below the waterline, the heave amplitude of DTP decreases, and the loads of the critical connections increase. A trade-off analysis for the elevation of LTP should be performed to find an optimized design of LTP elevation. However, as the telescopic columns and upper columns need to be connected offshore, designers will try to make the loads of local connections as low as possible. In such circumstances, an optimized solution should be found as the minimal LTP elevation below the waterline that could satisfy the requirements of the dry tree system.
(3) The analysis results will provide a basis for the engineering use of DTP concept.

Acknowledgments

This work is supported by China National Scientific and Technology Major Project (Grant No. 2011ZX05026), the scientific innovation program project by the Shanghai Committee of Science and Technology (Grant Nos. 14DZ1205501, 14DZ2250900 and 15DZ1207000) and the doctoral research fund of Shanghai Ocean University (A2-0203-00-100323). The model tests were executed at the State Key Laboratory of Ocean Engineering located in Shanghai Jiaotong University.

References

ABS, 2009. Guide for Building and Classing Floating Production Installations. American Bureau of Shipping.
Bennett, B., 2013. Proven alternative hull designs for surface drilling/production system, In: Proceedings of the Offshore Technology Conference. Houston, Texas, USA, OTC 23917.
Bindingsbø, A.U., Bjørset, A., 2002. Deep draft semi subm ersible. In: Proceedings of 21st International Conference on Offshore Mechanics and Arctic Engineering. ASME, Oslo, Norway.
Chakrabarti, S.K., Barnett, J., Kanchi, H., Mehta, A., Yim, J., 2007. Design analysis of a truss pontoon semi-submersible concept in deep water. Ocean Eng. 34, 621–629.
Colby C., SΦdahl N., et al., 2000. Coupling effects for a deepwater spar. In: Proceedings of the Offshore Technology Conference. Houston, Texas, USA, OTC 12082.
DNV, 2014. Sesam User Manual. Det Norske Veritas.
Gonçalves, R.T., Rosetti, G.F., Fujarra, A.L.C., Oliveira, A.C., 2012. Experimental study on vortex-induced motions of a semi-submersible platform with four square columns, Part I: effects of current incidence angle and hull appendages. Ocean Eng. 54, 150–169.
Gonçalves, R.T., Rosetti, G.F., Fujarra, A.L.C., Oliveira, A.C., 2013. Experimental study on vortex-induced motions of a semi-submersible platform with four square columns, Part II: effects of surface waves, external damping and draft condition. Ocean Eng. 62, 10–24.
Halkyard, J, Chao, J, Abbott, P, Dagleish J, Banon H, Thiagarajan K., 2002. A Deep Draft Semisubmersible with a Retractable Heave Plate. In: Proceedings of the Offshore Technology Conference, OTC-14304.
Haslum, H.A., Faltinsen, O.M., 1999. Alternative shape of Spar platform s for use in hostile areas. In: Proceedings of Offshore Technology Conference, Houston, USA.
He, H., 2003. Hydrodynamics of Thin Plates (Ph.D. thesis).. University of Michigan, United States.
Hansen V.L., Wang L., et al., 2004. Guidelines on coupled analyses of deepwater

floating systems. In: Proceedings of the Offshore Technology Conference Houston, Texas, USA, OTC 16588.
Holmes, S., Bhat, S., Beynet, P., Sablok, A., Prislin, I., 2001. Heave plate design with computational fluid dynamics. J. Offshore Mech. Arct. Eng. 123, 22–28.
Jiang Z., Xie B., Xie, W.H., Wang J.R., 2012. A Numerical investigation on the hydrodynamic performance of a new dry tree semisubmersible concept. In: Proceedings of the 22nd ISOPE Pacific/Asia Offshore Mechanics Symposium, Vladivostok, Russia.
Lake, M., He, H., Troesch, A., Perlin, M., Thiagarajan, K., 2000. Hydrodynamic coefficient estimation for TLP and Spar structures. J. Offshore Mech. Arct. Eng. 122, 118–124.
Magee, A., Sablok, A., Maher, J., Halkyard, J., Finn, L., Datta, I., 2000. Heaveplate effectiveness in the performance of truss Spars. In: Proceedings of the ETCE/OMAE2000 Joint Conference, New Orleans, LA, pp.1–11.
Mansour, A.M., 2009. FHS SEMI; a semisubmersible design for dry tree applications. In: Proceedings of the ASME 28th International Conference on Ocean, Offshore and Arctic Engineering, OMAE2009-79303.
Marintek, 2014a. RIFLEX Theory Manual, Marintek report.
Marintek, 2014b. SIMO Theory Manual, Marintek report.
Molin, B., 2001. On the added mass and damping of periodic arrays of fully or partially porous disks. J. Fluids Struct. 15, 275–290.
Murray, J.J., Yang, C.K., Chen, C.Y., Nah, E., 2008. Two dry tree semisubmersible designs for ultra deep water post-Katrina Gulf of Mexico, In: Proceedings of the ASME 27th International Conference on Ocean, Offshore and Arctic Engineering, OMAE2008-57462.
Newman, J.N., 1974. Second-order, slowly-varying forces on vessels in irregular waves. In: Proceedings of the International Symposium on the Dynamics of Marine Vehicles and Structures in Waves. University College, London.
Williams, N., Leverette, S., Bian, S., Large, S., Cao, P., 2010. Fourstar dry-tree semisubmersible development, In: Proceedings of the ASME 29th International Conference on Ocean, Offshore and Arctic Engineering, OMAE2010-20465.
Thiagarajan, K., Troesch, A., 1998. Effects of appendages and small currents on the hydrodynamic heave damping of TLP columns. J. Offshore Mech. Arct. Eng. 120, 37–42.
Thiagarajan, K., Datta, I., Ran, A., Tao, L., Halkyard, J., 2002. Influence of heave plate geometry on the heave response of classic spars. In: Proceedings of the 21st International Conference on Offshore Mechanics and Arctic Engineering. ASME. Oslo, Norway.
Prislin, I., Blevins, R., Halkyard, J., 1998. Viscous damping and added mass of solid square plates. In: Proceedings of the 17th International Conference on Offshore Mechanics and Arctic Engineering. ASME, Lisbon.
Shen, W., Tang, Y., Liu, L., 2012. Research on the hydrodynamic characteristics of heave plate structure with different form edges of a spar platform. China Ocean Eng. 26, 177–184.
Tao, L., Cai, S., 2004. Heave motion suppression of a spar with a heave plate. Ocean Eng. 31, 669–692.
Tao, L., Dray, D., 2008. Hydrodynamic performance of solid and porous heave plates. Ocean Eng. 35, 1006–1014.
Tao, L., Molin, B., Scolan, Y., Thiagarajan, K., 2007. Spacing effects on hydrodynamics of heave plates on offshore structures. J. Fluids Struct. 23, 1119–1136.
Xie, B., Xie, W.H., Jiang, Z., 2012. A new concept of a deepwater tumbler platform. In: Proceedings of the 22nd International Offshore and Polar Engineering Conference, Rhodes, Greece.